THE
AUSTRALIAN
NATIONAL
UNIVERSITY

RESEARCH SCHOOL OF PHYSICAL SCIENCES

ANU-P/786
December 1980

HIGH SPIN STATES AND YRAST ISOMERS IN ^{211}Rn

A.R. Poletti

Department of Physics, University of Auckland, New Zealand

G.D. Dracoulis and C. Fahlander

Department of Nuclear Physics, Australian National University,
Canberra, ACT 2600, Australia

and

I. Morrison

School of Physics, University of Melbourne, Victoria 3052, Australia

INSTITUTE OF ADVANCED STUDIES

ANU-P/786
December 1980

Accepted for publication in Nuclear Physics

HIGH SPIN STATES AND YRAST ISOMERS IN ^{211}Rn

A.R. Poletti

Department of Physics, University of Auckland, Private Bag,
Auckland, New Zealand

and

G.D. Dracoulis and C. Fahlander

Department of Nuclear Physics, Research School of Physical Sciences,
Australian National University, P.O. Box 4,
Canberra, A.C.T. 2600 Australia.

and

I. Morrison

School of Physics, University of Melbourne,
Parkville, Victoria 3052 Australia.

Abstract: Excited states in ^{211}Rn with spins up to 53/2 have been identified using (HI,xn) reactions and γ-ray techniques. A shell model calculation can reproduce the ordering of the yrast sequence up to spin $41/2^-$. Several yrast isomers have been identified. Enhanced E3 transitions are observed and their systematic occurrence in this region discussed. The influence of the neutron hole, and possible core excitations on the effective moment of inertia are also pointed out.

NUCLEAR REACTIONS ^{205}Tl(^{11}B,5n)^{211}Rn, E ~ 70 MeV; ^{198}Pt(^{18}O,5n)^{211}Rn, E ~ 95 MeV; measured γ-γ, neutron-γ prompt and delayed coincidences; E_γ, I_γ, $\gamma(\theta)$, ICC. ^{211}Rn deduced levels J, π, T, inferred configurations. Ge, Ge(Li), Ne213 detectors, enriched targets. Shell model calculation.

1. INTRODUCTION

The study of the structure of high spin states in nuclei near the Z = 82 and N = 126 closed shells is of considerable current interest. Metastable yrast states, or yrast traps, have been observed in this region, the highest spin examples being of states in ^{212}Rn[1,2]. In that case, aligned configurations with the four valence protons occupying the $h_{9/2}$, $i_{13/2}$ and $f_{7/2}$ orbitals dominate the yrast sequence up to spin 18, while at higher spins neutron core excitations play a significant, although not a well understood, role. The angular momentum alignment of high spin particle orbitals may lead, through a concentration of particles in the equatorial nuclear plane, to a preference for oblate deformation at high spin in these traditionally spherical nuclei. Matsuyanagi, Dossing and Neergard[3] calculate the yrast sequence in ^{212}Rn in a deformed basis and find that the development of oblate deformation is crucial to the understanding of the yrast spectrum. The presence of aligned hole configurations however will favour a prolate deformation, in competition with the particle excitations. This should be reflected in the structure of the yrast line both in terms of the level sequence and the appearance of yrast traps, and in the effective moment of inertia as deduced from the average slope of the excitation energy vs. I(I+1) curve.

This paper reports the first comprehensive study of states in ^{211}Rn, a nucleus with four valence protons and one neutron hole in the N = 126 shell. States with spins up to 53/2 have been identified and several isomers which qualify as yrast traps have been observed. The configurations of the observed states are discussed and compared with a shell model calculation, and with systematics in this region. The decay of the highest states by strongly enhanced E3 transitions is discussed with reference to similar transitions in neighbouring nuclei.

2. EXPERIMENTAL

Most of the information on the yrast states of ^{211}Rn was obtained using the ^{205}Tl(^{11}B,5n)^{211}Rn reaction at bombarding energies near 70 MeV. Some complementary measurements using the ^{198}Pt(^{18}O,5n)^{211}Rn reaction at energies near 95 MeV were also performed. The beams were provided by the ANU 14UD Pelletron accelerator. A variety of γ-ray spectroscopic techniques was used with both large volume Ge(Li) detectors and an intrinsic Ge LEPS detector to give sensitivity for high and low energy γ-rays. Detector efficiencies were measured using ^{152}Eu, ^{133}Ba and ^{125}Sb sources placed at the target position for each experimental geometry. Gamma-ray energies were deduced from simultaneous measurement of in-beam and source γ-rays. As well as γ-ray excitation functions, the experiments were:

2.1.1 γ-γ-time and neutron-γ-time. Multi-parameter event mode recording (EMR) of coincidence events using the ^{205}Tl(^{11}B,5n)^{211}Rn reaction with a rolled, self-supporting 13 mg/cm^2 enriched ^{205}Tl foil (^{205}Tl: 96.4%, ^{203}Tl: 3.6%). Two γ-ray detectors were placed at backward angles of about ± 135°, and the beam was stopped in a remote shielded beam dump. A neutron detector, (NE213 liquid scintillator) with pulse shape discrimination, detected fast neutrons at a forward angle, in coincidence with one of the γ-ray detectors. The time range used for both the γ-γ and neutron-γ coincidences was ± 4 μs since mean lives in the microsecond region were expected.

2.1.2 γ-γ-time and neutron-γ-time. A similar experiment to 2.1.1 was carried out using the ^{198}Pt(^{18}O,5n)^{211}Rn reaction with a high resolution intrinsic Ge LEPS detector together with a large Ge(Li) detector, both in close geometry at ± 90° to the beam direction. In this case the neutron-γ coincidences were taken with the LEPS detector. The target was a 4 mg/cm^2 enriched Pt foil (^{198}Pt: 95.8%, ^{196}Pt: 2.5%, ^{195}Pt: 1.2%) at 45° to the beam axis.

2.2 γ-ray angular distributions.

Two measurements were performed. The first used the $^{205}Tl + ^{11}B$ reaction with a remote beam dump. The angular range was 90° to 150°, and the yield was normalised to that in a second Ge(Li) detector fixed at 90° to the beam axis. The second measurement was with the $^{198}Pt + ^{18}O$ reaction. In this case the beam was stopped directly behind the 4 mg/cm^2 Pt target in a 0.13 mm thick Pb backing, and the angular range was 0° to 90°.

2.3 Neutron-γ anisotropy.

Since one of the main transitions in the ^{211}Rn yrast cascade was unresolved from the 511 keV annihilation γ-ray its anisotropy was measured at four angles between 90° and 150° in coincidence with the neutron detector. The γ-ray and time information was again recorded in event mode so that a measurement of each of the ^{211}Rn γ-rays was obtained. Improved timing information was also obtained by using slow rise-time rejection on the γ-ray pulses.

2.4 Conversion coefficients.

As well as the indirect determination of total conversion coefficients by intensity balances, especially from delayed intensities, electron conversion coefficients were measured directly. The in-beam electron spectrum was detected in a cooled Si(Li) detector at 125° to the beam direction, in conjunction with a "mini-orange" magnetic filter[4]. The γ-ray spectrum at 55° to the beam axis was recorded simultaneously. The target used was 3.5 mg/cm^2 ^{205}Tl evaporated on to a thin carbon foil placed at about 30° to the beam direction. The target thickness and angle were chosen as a compromise between electron resolution and the loss of recoiling nuclei. Electron and γ-ray efficiencies were measured (simultaneously) using ^{152}Eu, ^{207}Bi, ^{113}Sn, ^{137}Cs and ^{65}Zn sources.

3. RESULTS

3.1 Level scheme.

The position of the first excited state in ^{211}Rn is established at 540 keV both from the α-decay of ^{215}Ra[5]) and from the electron capture and positron decay of ^{211}Fr[6]). Two γ-rays at 120 and 918 keV were found to be in prompt coincidence (in this case prompt refers to a time range of ±150 ns) with the prominent 540 keV γ-ray. These three γ-rays were delayed with respect to a cascade of four strong γ-rays at 512, 570, 584 and 601 keV. A spectrum of γ-rays in coincidence with a delayed gate set on the 120, 540 and 918 keV γ-rays is shown in figure 1(a), with the complementary delayed spectrum in figure 1(b). These gates have been summed for convenience but the individual gates show the same features.

The two cascades preceding and following an isomer near 1578 keV account for the major part of the population in this region of the yrast sequence. The isomeric meanlife of 860±40ns deduced from both γ-γ and neutron-γ time spectra is attributed to an unobserved low energy transition feeding the 1578 keV state. All of our data are consistent with this hypothesis (including for example the presence of a prompt component in the time spectrum for the 120 keV transition), which follows the systematic occurrence of related states in ^{210}Rn[7]) and ^{212}Rn[1]). The very large conversion coefficients[8,9]) for low energy E2 transitions makes their observation difficult and from our measured efficiency for low energy transitions (which would allow us to observe unconverted γ-ray transitions down to about 25 keV) we place a limit of $\Delta < 50$ keV on the energy of this unobserved E2 transition.

A second, shorter-lived, isomer (58±2ns) decays by an 81.7 keV transition to the $3845 + \Delta$ keV state. This transition is almost resolved from the $K_{\alpha 2}$ Rn X-ray as shown in figure 2 where partial

low energy spectra in prompt coincidence with the (summed) 570, 584 and 601 keV gates and the (summed) 540 and 918 keV gates are compared. These last two transitions are below the 860ns isomer and therefore do not show the 81.7 keV transition in prompt coincidence. The placement of the 81.7 keV transition is supported by other coincidence data and by its time spectrum which shows the 58ns lifetime without a prompt component.

The ordering of the 601, 512, 584 and 570 keV transitions is based on their coincidence relationships with transitions not involved in the main cascade, on their intensities and relative excitation functions, and on the relative proportions of prompt and delayed components in their time spectra. A complication is introduced because of a second 584 keV transition higher in the level scheme, but this does not lead to ambiguities.

A third isomer with a lifetime of 41±4ns is established at 6101 + Δ keV, as shown in the decay scheme given in figure 3, and above this isomer a 1299 keV transition is observed. This and the remaining parts of the level scheme are assigned on the basis of the coincidence data, time spectra, relative excitation functions, energy summations and intensities. The energies of transitions assigned to ^{211}Rn are given in table 1. Several representative prompt coincidence spectra are shown in figure 4, and a number of time spectra are collected in figure 5. The measured lifetimes are summarised in table 2.

There are several uncertainties in the level scheme which should be stated explicitly. Firstly, the 537 keV transition is in prompt coincidence with the 601, 512 and 584 keV transitions indicating the existence of an unobserved 33 keV transition connecting the 2148 + Δ and 2115 + ΔkeV states. Secondly, the 411,325 keV cascade from the 5247 + Δ keV state

may be inverted. The ordering is difficult to establish because of the presence of a 325 keV transition in the side reaction leading to ^{210}Rn. Finally, the 730 keV transition which depopulates the 5241 + Δ keV state has a short lived component in its time spectrum, of a similar lifetime to that of the 6101 + Δ keV state, but the coincidence data do not establish a connection between the states, nor is any other isomeric feeding identified.

3.2 Spin assignments.

Spin and parity assignments were made on the basis of the angular distributions considered together with the conversion coefficients and lifetimes. The angular distribution data, and neutron-γ angular distributions, shown in Table 3, are less anisotropic than those usually observed in (Heavy ion, xn) reactions because of relaxation during the isomeric lifetimes, and this should be borne in mind when interpreting the anisotropies. The results from the ^{198}Pt + ^{18}O bombardment are not shown in the table because the attenuation in that case was found to be even larger, although the distributions were consistent with those from the ^{205}Tl + ^{11}B bombardment.

The conversion electron spectrum is given in figure 6, together with the corresponding singles γ-ray spectrum. The electron intensities were deduced by fitting measured lineshapes to the complex spectrum. Several strong activity lines present in these data were measured separately and provided useful internal checks both on the lineshapes, and on the efficiency measurements. Separate measurements were also made on the ^{205}Tl(^{10}B,5n)^{210}Rn reaction in a parallel study to that reported here[10], and those spectra provided a further check on contaminants

from ^{210}Rn, and on other contaminants in the γ-ray spectrum. The electron conversion coefficients for ^{211}Rn are summarised in table 4.

Briefly, the spin assignments were made as follows. Each of the cascade transitions below the 860ns isomer has a small positive A_2 coefficient consistent with attenuated stretched quadrupole transitions. This is confirmed by their measured conversion coefficients which are all close to the pure E2 values. This establishes, from the $1/2^-$ ground state, the $5/2^-$, $9/2^-$ and $13/2^-$ sequence. As stated earlier, the long lifetime is attributed to an unobserved E2 transition from the $17/2^-$ state. Similarly, above this isomer, the 570, 584, 512 and 601 keV transitions are respectively stretched quadrupoles and a stretched dipole, and the conversion coefficients assign E2 multipolarity for the first three, and E1 for the last. These assignments are also consistent with the absence of any lifetimes (a limit of < 5ns can be made from the γ-γ results) in this cascade. The 82 keV transition is assigned as a stretched E2 on the basis of its conversion coefficient and its lifetime.

Above the 58ns isomer, the 1320 keV transition which has a large positive A_2 coefficient and a small A_4 coefficient is assigned as a stretched E3 transition. Its conversion coefficient of $(0.70\pm0.11)\times10^{-2}$ is close to the theoretical value for an E3, (0.8×10^{-2}), and is inconsistent with a stretched M2 ($\alpha_K = 2.3\times10^{-2}$) or an E2 ($\alpha_K = 0.37\times10^{-2}$), both of which multipolarities are in any case unlikely because of the very large anisotropy. Although stretched quadrupole and octupole angular distributions both have positive A_2 coefficients[11,12], the A_2 for the 1320 keV transition is greater than the maximum obtainable from a completely aligned stretched quadrupole. The distribution coefficients A_L^M for fully aligned, high spin, stretched quadrupoles are about $A_2^M = +0.38$, $A_4^M = -0.13$ while for

octupoles $A_2^M = +0.68$, $A_4^M = +0.07$. Since the alignment will be partial (aside from attenuation due to relaxation), the observed values of $A_2 = +0.48(2)$, $A_4 = +0.04(2)$ are sufficient to eliminate the stretched quadrupole. Another unlikely possibility is a mixed M1/E2, J→J transition which could account for the conversion coefficient, but that would be inconsistent with the population of the 5247 + Δ keV state, as well as with that state's other branch cascading through the 4836 + Δ keV state, and with the relative excitation functions. All of these clearly identify the 5247 + Δ keV state as being of higher spin than the 3927 + Δ keV state. The 854 keV transition, which de-excites the 6101 + Δ keV state, is also assigned as a stretched E3 transition and in that case all the other (unlikely) possibilities are eliminated by the K/L conversion coefficient ratio. The 5247 + Δ and 6101 + Δ keV states are therefore assigned as $41/2^-$ and $47/2^+$ respectively.

Continuing up the main yrast sequence, the conversion coefficient of the 1299 keV transition also suggests an E3 transition, and its relative excitation function rises steeply compared to the 1320 and 854 keV transitions, consistent with a high spin for the 7400 + Δ keV state. Its angular distribution in the $^{11}B + ^{205}Tl$ reaction is also similar to that for the 1320 and 854 keV stretched E3 transitions, and therefore the 7400 + Δ keV state is assigned as $53/2^-$. In addition we note that in the angular distributions measured using the $^{18}O + ^{198}Pt$ reaction, in which more attenuation was observed than in the ^{11}B induced reaction, the A_2 coefficients were +0.13(2), +0.17(1) and +0.29(3) for the 1320, 854 and 1299 keV transitions respectively. The attenuation of the alignment is then least severe for the highest lying transition which has a mean life of <10ns, while the attenuation of the 854 and 1320 keV transitions is larger because of the 41ns mean life of the 6101 + Δ keV state.

Returning to the lower states, the weakly populated 2651 + Δ and

3118 + Δ keV states are assigned as 23/2 and 25/2 respectively from the dipole angular distributions of the 503 and 467 keV γ-rays. Unfortunately, only a limit is obtained for the 503 keV conversion coefficient, and the limit in this case is not sufficient to distinguish between E1 and M1 multipolarities. The 467 keV transition is assigned as mainly M1. The large anisotropy suggests a mixed M1/E2 transition which is consistent with an E2 admixture of about 8% required by the measured conversion coefficient.

Finally, an assignment of $37/2^+$ is made to the 4511 + Δ keV state, and the 411 and 325 keV cascade transitions which feed it are respectively M1 and E1. Although the 325 keV γ-ray is contaminated by a transition of the same energy in ^{210}Rn, that transition is a known stretched quadrupole. The small negative A_2 coefficient for the combined ^{210}Rn and ^{211}Rn transitions therefore suggests a larger negative A_2, and therefore a dipole character, for the ^{211}Rn component. The limit on the conversion coefficient is sufficient to eliminate the M1 possibility because of the large difference between E1 and M1 coefficients[8]. Depending on the ordering of the 325 and the 411 keV transitions, the intermediate state of spin 39/2 has either negative or positive parity. The 730 keV transition is a stretched dipole and from the conversion coefficient has multipolarity E1, giving a $39/2^-$ assignment for the 5241 + Δ keV state.

The above assignments are consistent with, and supported by, the lifetime measurements and limits. The cascade of enhanced E3 transitions in the high spin sequence will be discussed in section 5.2.

4. SHELL MODEL CALCULATION

In order to assist in the elucidation of the configurations of yrast states in ^{211}Rn, the level spectrum was calculated in the framework of the shell model using the Glasgow shell model code[13]. It is not appropriate to give a full description of the calculations here since they are part of a wider study of nuclei in the lead region[14], so only a brief outline is given.

It was necessary to restrict the basis states to those involving the four valence protons in the $1h_{9/2}$, $2f_{7/2}$ and $1i_{13/2}$ orbitals, and the neutron hole in the $3p_{1/2}$, $3p_{3/2}$ and $2f_{5/2}$ orbital. From a consideration of the single particle energies[15,16], and from the spectrum of ^{212}Rn[1,2], which was also calculated in the model, the truncation is expected to be severe in the region of spin 20 and above. The main configurations which will intrude in this region are those involving the $1i_{13/2}$ neutron hole, and core excited configurations where a neutron is promoted across the N = 126 shell, particularly to the $2g_{9/2}$ orbit.

The parameters of the calculation were chosen to give a reasonable reproduction of the ^{210}Po and ^{208}Bi level schemes, and after that no further adjustments were made. The single particle and hole energies were taken from experiment[15,16]. The modified surface delta interaction[17] with strength parameter A_1 = 0.159, which reproduces the excitation energy of the first 2^+ state in ^{210}Po, was used for the proton-proton interaction. This interaction was used by Arvieu in calculations for ^{211}At and well reproduces the low-lying and yrast levels in that nucleus[18]. It also reproduces the low spin spectrum of ^{212}Rn[14], and is consistent with the results of McGrory and Kuo[19] who use an interaction derived from

perturbation theory. For spins >8 in ^{212}Rn, the calculated yrast levels are in the correct sequence but are uniformly depressed by ~200 keV in comparison with experiment, and that will necessarily also be the case in ^{211}Rn. A quadrupole-quadrupole interaction chosen to give a reasonable fit to the spectrum of ^{208}Bi was used for the proton particle-neutron hole interaction. This gave average two-body matrix elements of about 50 keV.

The calculated yrast, and the lowest non yrast states in ^{211}Rn are compared with experiment in figure 7. The main configurations are also shown in the figure, as is the experimental scheme for ^{212}Rn[1]. Although there is significant mixing between different configurations, each state is still dominated by a particular configuration, being between 70% pure for the lower spin states, and about 95% pure for particular high spin states.

5. DISCUSSION

5.1 Comparison with shell model calculation and with ^{212}Rn.

As can be seen from figure 7, allowing for the compression of the calculated spectrum, there is a good correspondence between the calculated and experimental yrast states up to the $41/2^-$ state. For example, the close doublet of states with spins $31/2^+$ and $35/2^+$ observed experimentally at about 3.9 MeV are reproduced in the calculation. Further, the experimental B(E2) of 176 e^2fm^4 for the 82 keV transition connecting these states is in fair agreement with the predicted value of 64 e^2fm^4, calculated using effective proton and neutron charges of 1.5 and 1.0 respectively. This proton effective charge approximately reproduces transition strengths in ^{210}Po, ^{211}At and ^{212}Rn, while the neutron effective charge is chosen from fits to the lead isotopes $^{204-207}$Pb [14]. There is also good correspondence between the experimental ^{211}Rn and ^{212}Rn schemes, with the addition of the appropriate neutron hole, up to the $41/2^-$ ^{211}Rn state at 5247 + Δ keV, which is associated with the yrast (20^+) state in ^{212}Rn at 5403 keV. Correspondingly, the dominant configurations given in figure 7 for ^{211}Rn, as given by the shell model calculations, agree with those given in the calculation of Blomqvist[1,20] for ^{212}Rn.

At higher spins however, both experimental and theoretical comparisons fail. In the shell model calculation there are no counterparts for the observed $47/2^+$ isomeric state, and for the $53/2^-$ state. The first calculated $47/2^+$ state, from the $\pi[h_{9/2}\, i^3_{13/2}]\nu f^{-1}_{5/2}$ configuration, is 1.5 MeV higher than the observed state, in contrast to the usual underestimate of the excitation energy. As stated earlier, the restricted basis is likely to be at fault in this spin region, and we note that in ^{212}Rn, the states which are yrast in this region are

believed to be core excited configurations[1,2].

However, if we compare the ^{211}Rn and ^{212}Rn experimental schemes there is a marked difference above the $41/2^-$ and 20^+ yrast states of the two nuclei. In ^{212}Rn, the main decay proceeds through states (for example the non yrast 20^+ state at 6180 keV) which do not have counterparts in ^{211}Rn. The yrast 22^+, 25^-, 27^- and 30^+ states in ^{212}Rn probably have core excited configurations, but corresponding states, obtained by adding an aligned $p_{1/2}$ or $f_{5/2}$ neutron hole, are not seen in ^{211}Rn. This lack of correspondence, in contrast to that observed at lower spins, may be a direct result of the onset of deformation in ^{212}Rn associated with particular core excitations which have two neutron holes coupled to spin zero, and therefore will not have counterparts in ^{211}Rn. These and related points will be discussed further below.

One feature of both the ^{211}Rn and ^{212}Rn schemes which bears directly on the question of configurations is the presence of enhanced E3 transitions between particular high spin states. In ^{211}Rn, for example, the $41/2^-$ state decays by an enhanced 1320 keV E3 of > 3 s.p.u., and a similar transition is observed in ^{212}Rn. From the assigned configurations the transition involved is essentially the proton $\pi i_{13/2}$ to $\pi h_{9/2}$, which is expected to be enhanced[20], lending support to the assignments. Since the two higher transitions in the ^{211}Rn scheme are also enhanced E3's, it is instructive to compare these with other E3 transitions in neighbouring nuclei.

5.2 Enhanced E3 transitions and yrast configurations.

Enhanced E3 transitions are well known in the lead region, and they can usually be associated with the coupling of the octupole mode with specific particle transitions[21,22]. The $53/2^-$ to $47/2^+$, and $47/2^+$ to $41/2^-$ transitions in ^{211}Rn have strengths of > 11 and 49 s.p.u. respectively, comparable to the 29 s.p.u. found for decay of the 3^- octupole state in ^{208}Pb. A selection of E3 transitions from ^{212}Rn[1,2], ^{211}Rn, ^{210}Rn[10], ^{209}At[23], ^{210}At[24] and ^{211}At[25,26] are illustrated in figure 8, with their partial decays, and suggested state configurations. As has been pointed out previously, particular particle transitions (the proton $\pi i_{13/2}$ to $\pi f_{7/2}$ and $\pi i_{13/2}$ to $\pi h_{9/2}$, and the neutron $\nu j_{15/2}$ to $\nu g_{9/2}$ transitions) give rise to enhanced octupoles[24]. In ^{211}At for example, the $29/2^+$ to $23/2^-$ transition of 19 s.p.u. can be attributed to the $\pi i_{13/2}$ to $\pi f_{7/2}$ transition[25]. In ^{209}Bi the related transition is calculated to be about 30 s.p.u.[22]. The $\pi i_{13/2}$ to $\pi h_{9/2}$ transition in ^{209}Bi is weaker, about 6 s.p.u.[27], and comparable transitions are observed in the decay of the 20^+ state in ^{210}Rn[10], and the $41/2^-$ state in ^{211}Rn, in agreement with the proposed configurations. Unfortunately the strength of the corresponding 20^+ to 17^- transition in ^{212}Rn is not known because no lifetime is reported for the (20^+) state[2]. However, we can infer a limit on that lifetime which would lead to a similar E3 strength.

In general, from figure 8, comparable enhanced E3 transitions can be associated with specific one-particle transitions, although the transition strengths between the high spin states which involve core excited configurations are somewhat larger. The question that arises therefore is whether the proposed configurations for the higher spin yrast states

in ^{212}Rn and ^{211}Rn are consistent with the observed E3 strengths. For example, the 25^- to 22^+ transition in ^{212}Rn of 32 s.p.u. is mainly a $\pi i_{13/2}$ to $\pi h_{9/2}$ transition according to the configurations assigned by Matsuyanagi, Dossing and Neergard[3], and Anderson et al.[28]. This is larger than the expected transition strength, due probably to polarisation effects in these core excited states which are susceptible to deformation. However, in the same nucleus, the configurations suggested by those authors for the 30^+ and 27^- states involve a change of both a proton and a neutron orbit, which would not therefore lead to a strong transition. In contrast the experimental transition is 36 s.p.u.

In ^{211}Rn we have not as yet proposed configurations for the $47/2^+$ and $53/2^-$ yrast states since configurations which satisfy both the criteria of excitation energy and enhanced E3 transition rates (the $47/2^+$ to $41/2^-$ strength is 49 s.p.u.), do not immediately suggest themselves. The possible configurations are further constrained because, as shown earlier, the configuration of the $41/2^-$ state to which the $47/2^+$ state decays is at least predominantly the $(h^2_{9/2}\, i^2_{13/2})_{20^+}\, \nu p^{-1}_{1/2}$ configuration.

One possibility is that there is a significant admixture of the $\pi[h^3_{9/2}f_{7/2}]_{13}$-$\nu(p^{-2}_{1/2})_0 g_{9/2}$ configuration in the $35/2^+$, 3927 + Δ keV state, a $\pi[h^2_{9/2}f_{7/2}i_{13/2}]_{16}$- $\nu(p^{-2}_{1/2})_0 g_{9/2}$ component in the $41/2^-$ state, and that

the $47/2^+$ and $53/2^-$ states are mainly from the $\pi[h_{9/2}^2 i_{13/2}^2]_{19^+} \nu(p_{1/2}^{-2})\, g_{9/2}$ and $\pi[h_{9/2}^2 i_{13/2}^2]_{19^+} \nu(p_{1/2}^{-2})_0 j_{15/2}$ configurations respectively. This would then provide the appropriate sequence of enhanced one-particle E3 transitions with spectator groups of nucleons. Although excitation of the extra neutron across the N = 126 gap is at first sight expensive in terms of energy, it has been stressed that deformations will play a role at these high spins[3,28], and that the $g_{9/2}$ neutron orbit decreases steeply in energy as a function of oblate deformation. A related fact is that the core excitations involving the $\nu p_{1/2}^{-1} g_{9/2}$ excitation (a number of which are shown in figure 8) are depressed in energy by up to 1 MeV[1,29].

Our hesitancy in assigning these configurations comes partly from our estimate that even larger energy depressions would be required to bring these configurations low enough in energy, and that the suggested configurations of the $47/2^+$ and $53/2^-$ states would have non-stretched proton components ($\pi[h_{9/2}^2 i_{13/2}^2]$ coupled to 19^+ rather than the maximum 20^+). This second point assumes that the $g_{9/2}$ neutron hole would be aligned. The elucidation of the configurations of the highest states in ^{211}Rn, and as pointed out earlier, in ^{212}Rn, remains an open problem.

The presence of enhanced E3 transitions can be seen as a general feature of the decay of high spin yrast states in this region, and it warrants a general explanation. Bohr and Mottelson[21] have pointed out, in their generalisation of nuclear shell structure, that the presence of a number of close lying pairs of orbitals such as the $i_{13/2}$ and $f_{7/2}$ protons, and the $j_{15/2}$ and $g_{9/2}$ neutrons will lead to enhanced E3 transitions, and even further, to a preference for deformations with an octupole asymmetry. A related discussion is given by Sheline[30].

It is unlikely that this will lead to a static octupole deformation, but rather to a coupling between quadrupole and octupole phonons. Vogel[31] has also discussed this point, and he shows that in potential energy surface calculations (not however for high spin) in the radon region the minimum energy is obtained for a zero static octupole deformation (β_3), but that the surface relating quadrupole (β_2) and β_3 deformations is shallower for $\beta_2 < 0$ than for $\beta_2 > 0$. This can be understood intuitively from the point of view that an oblate deformed shape could be the first step (from sphericity) in the onset of an octupole oscillation about the same axis. The inclusion of β_3 as well as β_2 deformations in high spin calculations would be a useful step in understanding the E3 transitions. The presence of the same E3 transitions may also indirectly provide support for the suggestion that a transition to oblate deformation occurs at high spin in these nuclei, as will be further discussed in the next section.

5.3. Effective Moment of Inertia.

From the calculations of Matsuyanagi, Dossing and Neergard[3], and Andersson et al.[28], oblate deformation is expected to be important for the high spin yrast states. Andersson et al.[28], for example, identify the 19^+ isomer in ^{210}At (the isotone of ^{211}Rn) as the "band head" of the oblate deformed band. For this state, and in general, oblate deformation is favoured by neutron core excitations which populate the neutron orbitals ($g_{9/2}$,$i_{11/2}$,$j_{15/2}$) above the N = 126 closed shell. In turn these states are "stabilised" by the deformation and are expected to figure in the yrast sequence and also to produce yrast traps. The alignment of particle angular momentum plays a key role since it implies the concentration of particles in the equatorial plane, and therefore oblate deformation. In contrast the alignment of neutron holes favours

a prolate deformation. Hence, configurations which contain both aligned high spin particles and high spin holes (e.g. in ^{211}Rn, the $\nu i^{-1}_{13/2}$ neutron hole), are unlikely to compete in the yrast region if deformation is important. In this context we note that the highest spin (low energy) aligned proton configuration is $\pi[h^2_{9/2}i^2_{13/2}]$, coupled to a maximum spin of 20 $\hbar$.

In the absence of deformation and core excitation, the energy required for a given angular momentum will depend on the number of valence particles, and it is useful to discuss the relationship between excitation energy and angular momentum in terms of the effective moment of inertia. The more particles available for alignment, the less energy required for a given angular momentum, hence the larger the effective moment of inertia. Horn et al.[2] discuss this point, and for ^{212}Rn they show that there is a change from a relatively low moment of inertia ($2\mathcal{J}/\hbar^2 \simeq 85$ MeV^{-1}), which is attributed to the four valence protons, to a higher value of 191 ± 4 MeV^{-1}, which is close to the rigid body value. The change occurs where core excited states intrude into the yrast sequence. The effective moments of inertia as deduced from a least squares fit naturally depend on which states are included, and we note that if the yrast (20^+) state in ^{212}Rn were included in the extraction of either the lower or upper regions given in figure 9, the difference between the two moments of inertia would be less dramatic. The yrast states in ^{211}Rn are compared with ^{212}Rn in figure 9. The effective moment of inertia in ^{211}Rn deduced from the states with spins 9/2 to 41/2 is 107 ± 3 MeV^{-1}, significantly larger than that for ^{212}Rn. This can be understood as the effect of the extra valence particle, the neutron hole, providing angular momentum for alignment. The difference in slope corresponds to about $\lesssim 2$ units of angular momentum being available, consistent with the contribution of the $p_{1/2}$ and $f_{5/2}$ neutron holes. At higher spins the yrast slope deviates to give a moment of inertia of about 140 MeV^{-1}. This is considerably less than

that in ^{212}Rn, although, because of the small number of points, there is considerable uncertainty in the ^{211}Rn case. Nevertheless, there is a definite change at or near spin $41/2^-$, and from the discussion in section 5.2, this is where we expect at least admixtures of core excited (and by implication, deformed) states to become important.

Extension of the yrast sequence in ^{211}Rn to still higher spins is important to allow a definitive statement on whether the equivalent changes in the yrast states of ^{211}Rn and ^{212}Rn occur.

6. SUMMARY

The level scheme of ^{211}Rn, of which little was known previously, has been established up to spin 53/2. The configurations of most of the states up to the $41/2^-$ yrast state are identified with reference to a shell model calculation. The configurations of the higher states which decay by enhanced E3 transitions remain an open question, although some suggestions for core excited configurations have been made. The effective moment of inertia of the yrast sequence is consistent with that observed in ^{212}Rn, with the addition of the effect of a valence neutron hole. At high spins a change in the slope is observed, indicating the possible influence of deformed states, but extension to still higher spins is required.

ACKNOWLEDGEMENTS

We would like to thank the academic and technical staff of the ANU 14UD accelerator facility for their support in this work. In particular we are grateful to Dr. M.P. Fewell who participated in the earlier measurements, Dr. I.G. Graham for computer program development and A. Muggleton for target preparation. A.R.P. acknowledges the support of the University of Auckland Research Committee.

REFERENCES

1) D. Horn, O. Häusser, T. Faestermann, A.B. McDonald, T.K. Alexander, J.R. Beene and C.J. Herrlander, Phys.Rev.Lett. 39 (1977) 389.

2) D. Horn, O. Häusser, B. Haas, T.K. Alexander, T. Faestermann, H.R. Andrews and D. Ward, Nucl.Phys. A317 (1979) 520.

3) K. Matsuyanagi, T. Døssing and K. Neergård, Nucl. Phys. A307 (1978) 253.

4) M. Ishii, Nucl.Instr. & Meth. 127 (1975) 53.

5) D.F. Torgerson and R.D. Macfarlane, Phys.Rev. C2 (1970) 2309.

6) T. Kempisty, A. Korman, T. Morek, L.K. Peker, Z. Haratym and S. Chojnacki, Joint Institute for Nuclear Research (Dubna) Report JINR-P6-6723 (1972).

7) A.R. Poletti, T.P. Sjoreen, D.B. Fossan, U. Garg, A. Neskakis and E.K. Warburton, Phys.Rev. C20 (1979) 1768.

8) R.S. Hager and E.C. Seltzer, Nuclear Data A4 (1968) 1.

9) O. Dragoun, Z. Plajner and F. Schmultzler, Nuclear Data A9 (1971) 119.

10) A.R. Poletti, G.D. Dracoulis and C. Fahlander, to be published.

11) T. Yamazaki, Nuclear Data A 13 (1967) 1.

12) E. der Mateosian and A.W. Sunyar, Atomic and Nuclear Data Tables 13 (1974) 391, 407.

13) R.R. Whitehead, A. Watt, B.J. Cole and I. Morrison, Advances in Nucl. Phys. 9 (1977) 123, ed. M. Baranger, E. Vogt (Plenum Press).

14) I. Morrison, to be published.

15) A. Bohr and B.R. Mottelson, "Nuclear Structure" Vol.I, p.324 (W.A. Benjamin, New York, 1969).

16) C.M. Lederer and V.S. Shirley, editors, "Table of Isotopes", 7th Edition (John Wiley & Sons, 1978).

17) P.W.M. Glaudemans, P.J. Brussaard and B.H. Wildenthal, Nucl.Phys. A102 (1967) 593.

18) R. Arvieu, O. Bohigas and C. Quesne, Nucl.Phys. A143 (1970) 577.

19) J.B. McGrory and T.T.S. Kuo, Nucl.Phys. A247 (1975) 283.

20) J. Blomqvist, Proceedings of the Symposium on "High-Spin Phenomena in Nuclei" Argonne 1979 ANL-PHYS-79-4 p.155.

21) A. Bohr and B.R. Mottelson, "Nuclear Structure" Vol.II (W.A. Benjamin, 1975); B.R. Mottelson, Nikko Summer School Lectures 1967.

22) P. Ring, R. Bauer and J. Speth, Nucl.Phys. A206 (1973) 97.

23) I. Bergström, C.J. Herrlander, Th. Lindblad, V. Rahkonen, K-G Rensfelt and K. Westerberg, Z.Physik A273 (1975) 291.

24) V. Rahkonen, I. Bergström, J. Blomqvist, O. Knuuttila, K-G Rensfelt, J. Sztarkier and K. Westerberg, Z.Physik A284 (1978) 357.

25) I. Bergström, B. Fant, C.J. Herrlander, K. Wikström and J. Blomqvist, Physica Scripta 1 (1970) 243,

26) K.H. Maier, J.R. Leigh, F. Pülhofer and R.M. Diamond, Phys.Lett. 35B (1971) 401.

27) J.R. Beene, O. Häusser, T.K. Alexander and A.B. McDonald, Phys.Rev. C17 (1978) 1359.

28) C.G. Andersson, G. Hellström, G. Leander, I. Ragnarsson, S. Åberg, J. Krumlinde, S.G. Nilsson and Z. Szymanski, Nucl.Phys. A309 (1978) 141.

29) D. Horn, O. Häusser, T. Faestermann, A.B. McDonald, T.K. Alexander, J.R. Beene and C.J. Herrlander, Proc.Int.Conf. Nuclear Structure, Tokyo 1977, J.Phys.Soc.Japan 44 (1978) Suppl.p.605.

30) R.K. Sheline, Phys.Rev. C21 (1980) 1660.

31) P. Vogel, Nucl.Phys. A112 (1968) 583.

TABLE 1

Energies and placement of γ-rays in ^{212}Rn.

Energy (keV)	Initial State[a)]	Final State[a)]
81.7(2)	3927 + Δ	3845 + Δ
119.6(1)	1578	1458
325.1(2)[b]	4836 + Δ	4511 + Δ
411.0(2)[b]	5247 + Δ	4836 + Δ
466.6(2)	3118 + Δ	2651 + Δ
502.9(1)	2651 + Δ	2148 + Δ
511.5(1)	3244 + Δ	2732 + Δ
536.1(2)	2114 + Δ	1578 + Δ
539.9(1)	540	0
569.9(1)	2148 + Δ	1578 + Δ
583.6(2)	4511 + Δ	3927 + Δ
584.2(1)	2732 + Δ	2148 + Δ
601.0(1)	3845 + Δ	3244 + Δ
730.2(1)	5241 + Δ	4511 + Δ
854.1(1)	6101 + Δ	5247 + Δ
918.3(1)	1458	540
1298.6(2)	7400 + Δ	6101 + Δ
1319.9(2)	5247 + Δ	3927 + Δ

a) Δ is the energy of the unobserved $17/2^- \rightarrow 13/2^-$ transition which is < 50 keV.

b) See text; the ordering of these transitions may be reversed.

TABLE 2

Summary of lifetimes, and limits on the lifetimes of states in ^{211}Rn

Level (keV)	Mean Life (ns)	γ-rays
1578 + Δ	860 ± 40	120,918,540
3927 + Δ	58 ± 2	82,601,512,584,570
6101 + Δ	41 ± 4	854,1320,325,411
	Lifetime Limit (ns)	**Source**
540	≤ 5	γ-γ coincidences
2148 + Δ	≤ 5	"
2732 + Δ	≤ 5	"
3244 + Δ	≤ 5	"
3845 + Δ	≤ 10	neutron-γ
5241 + Δ[a)]	≤ 10	neutron-γ 730 keV transition[a)]
5247 + Δ	≤ 25	"
7400 + Δ	≤ 10	"

a) an unassigned delayed component with a mean life of ∿ 50 ns feeds this level.

TABLE 3

Angular distributions and intensities of γ-rays in ^{211}Rn from the ^{205}Tl(^{11}B,5n)^{211}Rn reaction at 72 MeV. The parameters A_2/A_0 and A_4/A_0 are the coefficients of the Legendre polynomial expansion. The last two columns give these coefficients as deduced from the neutron-γ anisotropy measurements.

		Singles		Neutron-γ	
E_γ (keV)	Intensity	A_2/A_0	A_4/A_0	A_2/A_0	A_4/A_0
82	22(4)				
120	91(5)	+0.08(1)	-0.07(2)		
325	∿ 44[a]	-0.02(1)	-0.02(2)	-0.05(3)	0.07(5)
411	36(4)	-0.26(2)	-.03(3)	-0.29(4)	0.00(7)
467	25(3)	-0.79(4)	0.09(6)		
503	36(4)	-0.15(4)	0.00(5)	-0.18(9)	-0.16(16)
512[b]	∿ 198[b]	0.00(1)	-0.01(2)	0.13(1)	0.01(2)
536	61(6)	-0.10(2)	0.21(3)	-0.20(4)	0.03(6)
540	416(20)	0.09(1)	-0.02(1)		
570	259(12)	0.28(1)	-0.07(1)	0.21(1)	-0.03(2)
583.6	36(5)	-0.48(8)	0.00(11)		
584.2	272(14)	0.19(1)	-0.06(1)		
601	199(10)	-0.11(1)	0.01(2)	-0.17(1)	0.02(2)
730	31(3)	-0.13(3)	0.05(4)	-0.09(7)	0.03(10)
854	68(5)	0.40(2)	-0.03(2)	0.29(3)	-0.01(5)
918	418(20)	0.10(1)	-0.03(1)		
1299	24(4)	0.40(4)	-0.04(6)	0.39(10)	0.05(17)
1320	48(5)	0.48(2)	-0.02(4)	0.38(5)	0.14(8)

a) Singles intensity corrected for the contaminant 325 keV line from ^{210}Rn; the angular distribution is for the sum of the two components.

b) Singles intensity corrected for the annihilation contaminant. The singles angular distribution contains this contaminant, the n-γ anisotropy will only have a small annihilation component.

TABLE 4

Summary of conversion coefficient measurements in ^{211}Rn

E_γ (keV)	Type[a]	Experiment α	Multi-polarity	Theory α[b]
82	T	$>10.5 \pm 1.7$	E2	21
120	T	4.3 ± 0.4	E2	4.0
325 [c]	K	$\leq 2.3 \times 10^{-2}$ [c]	E1	2.2×10^{-2}
411	K	0.27 ± 0.03	M1	0.22
467	K	0.17 ± 0.02	M1	0.15
503	K	$\leq 2.3 \times 10^{-2}$		
512 [d]	K	$(2.4 \pm 0.3) \times 10^{-2}$ [d]	E2	2.3×10^{-2}
540	K	$(2.4 \pm 0.3) \times 10^{-2}$	E2	2.1×10^{-2}
570	K	$(1.9 \pm 0.2) \times 10^{-2}$	E2	1.9×10^{-2}
583.6	K	$(2.9 \pm 0.3) \times 10^{-2}$ [e]	E2+M1	2.7×10^{-2} [e]
584.2	L	$(0.71 \pm 0.12) \times 10^{-2}$	"	0.69×10^{-2}
601	K	$(0.53 \pm 0.08) \times 10^{-2}$	E1	0.63×10^{-2}
730	K	$< 0.5 \times 10^{-2}$	E1	0.44×10^{-2}
854	K	$(1.98 \pm 0.18) \times 10^{-2}$ [f]	E3	1.9×10^{-2}
	L	$(0.59 \pm 0.13) \times 10^{-2}$	"	0.70×10^{-2}
918	K	$(0.71 \pm 0.09) \times 10^{-2}$	E2	0.70×10^{-2}
	L	$(0.16 \pm 0.03) \times 10^{-2}$	"	0.14×10^{-2}
1298	K	$(0.99 \pm 0.12) \times 10^{-2}$	E3	0.83×10^{-2}
1320	K	$(0.70 \pm 0.11) \times 10^{-2}$	E3	0.80×10^{-2}

a) T: total ICC deduced from intensity balances; K,L: direct measurements of α_K, α_L.

b) Ref.[8,9].

c) Corrected for the intensity of the 325 keV transition in ^{210}Rn.

d) γ-ray intensity corrected for the 511 annihilation line.

e) Two transitions present; the theoretical value assumes E2 for the main component and M1 for the other, with relative intensities as given in table 3.

f) Corrected for a small activity contaminant.

FIGURE CAPTIONS

Fig. 1(a) Spectrum of "early" γ-rays in coincidence with the 120, 540 and 918 keV transitions with a delayed gate of 155 to 1580 ns.

1(b) Spectrum of delayed γ-rays in coincidence with the 570, 584 and 601 keV lines.

Fig. 2. Partial prompt coincidence spectra recorded in the LEPS detector showing the 81.7 keV transition, partially resolved from the Rn K_{α_2} X-ray.

Fig. 3. Level scheme determined in this work. The width of the shaded transitions represents the γ-ray intensity observed in the $^{205}Tl + ^{11}B$ reaction.

Fig. 4. Representative prompt γ-ray coincidence spectra.

Fig. 5. Representative time spectra from neutron-γ coincidences.

Fig. 6(a),(b) Singles γ-ray spectrum, and electron spectrum, from the $^{11}B + ^{205}Tl$ reaction with the "mini-orange" spectrometer. A number of contaminant γ-rays are present due mainly to inelastic neutron scattering in the "mini-orange" target chamber material which are not present in the other (singles and coincidence) γ-ray measurements.

Fig. 7. Comparison between the shell model calculations described in the text, the ^{211}Rn experimental scheme, and the ^{212}Rn scheme[1,2]. The configurations shown for ^{211}Rn are the dominant configuration. The dashed lines connect levels in ^{211}Rn and ^{212}Rn which are related by the addition of a neutron hole. The levels on the left of the theoretical ^{211}Rn scheme are near-yrast states which would not be strongly populated in this study.

Fig. 8. Comparison of enhanced E3 transitions in ^{211}Rn (this work) ^{212}Rn[1,2], ^{210}Rn[10], ^{209}At[23], ^{210}At[24] and ^{211}At[25,26]. The configurations shown are the dominant configurations, and discussion of important admixtures is contained in the original references. The transition strengths in single particle units are given in parentheses after the transition energy.

Fig. 9. Plot of excitation energy vs. I(I+1) for states in ^{210}Rn and ^{211}Rn. For ^{212}Rn the two curves are those of Horn et al.[2]. The yrast spin 20 state in that nucleus discussed in the text is indicated by a crossed open circle.

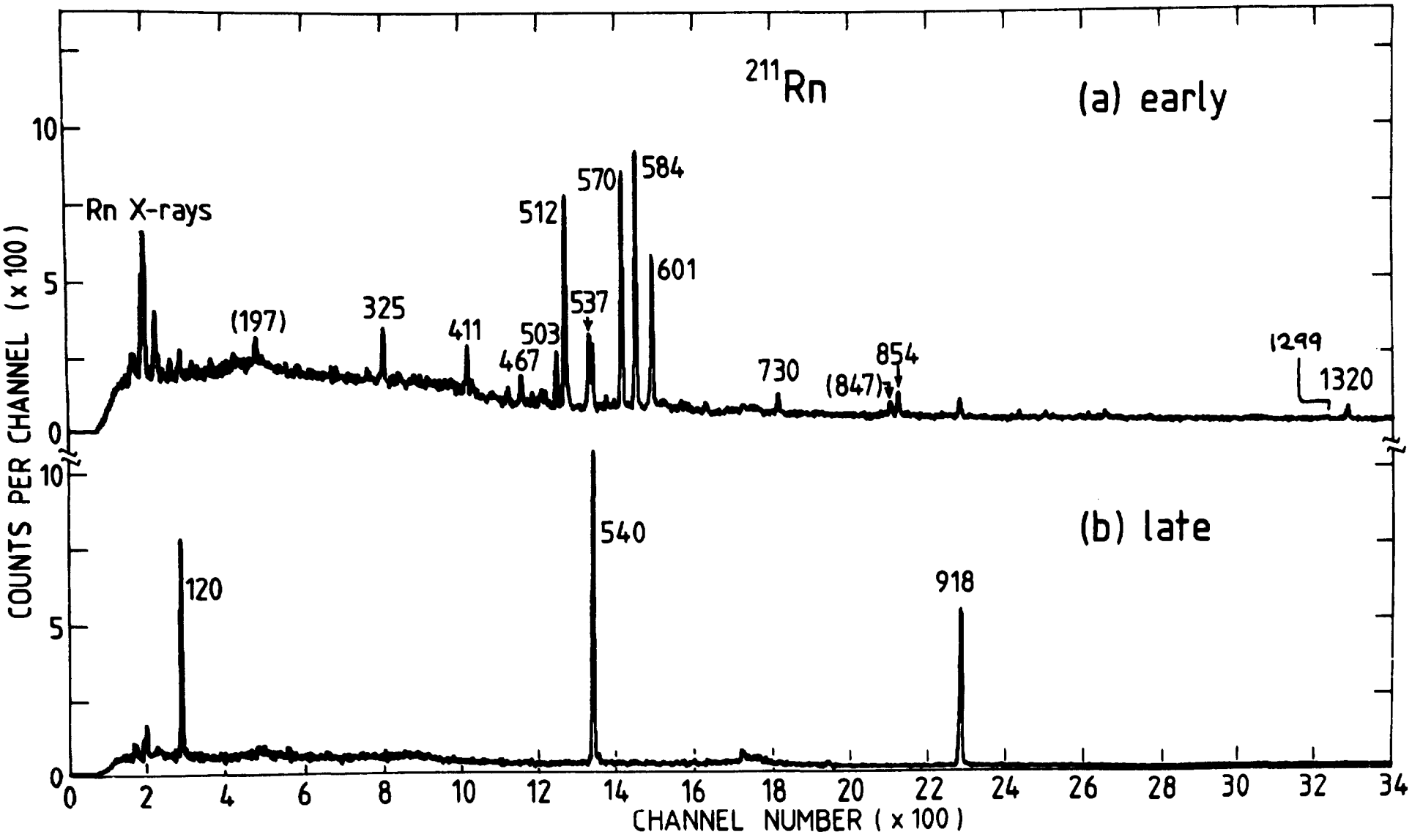
211Rn
(a) early
Rn X-rays
(197)
325
411
503
467
512
537
570
584
601
730
(847)
854
1299
1320
(b) late
120
540
918
COUNTS PER CHANNEL (x 100)
CHANNEL NUMBER (x 100)

Fig. 1

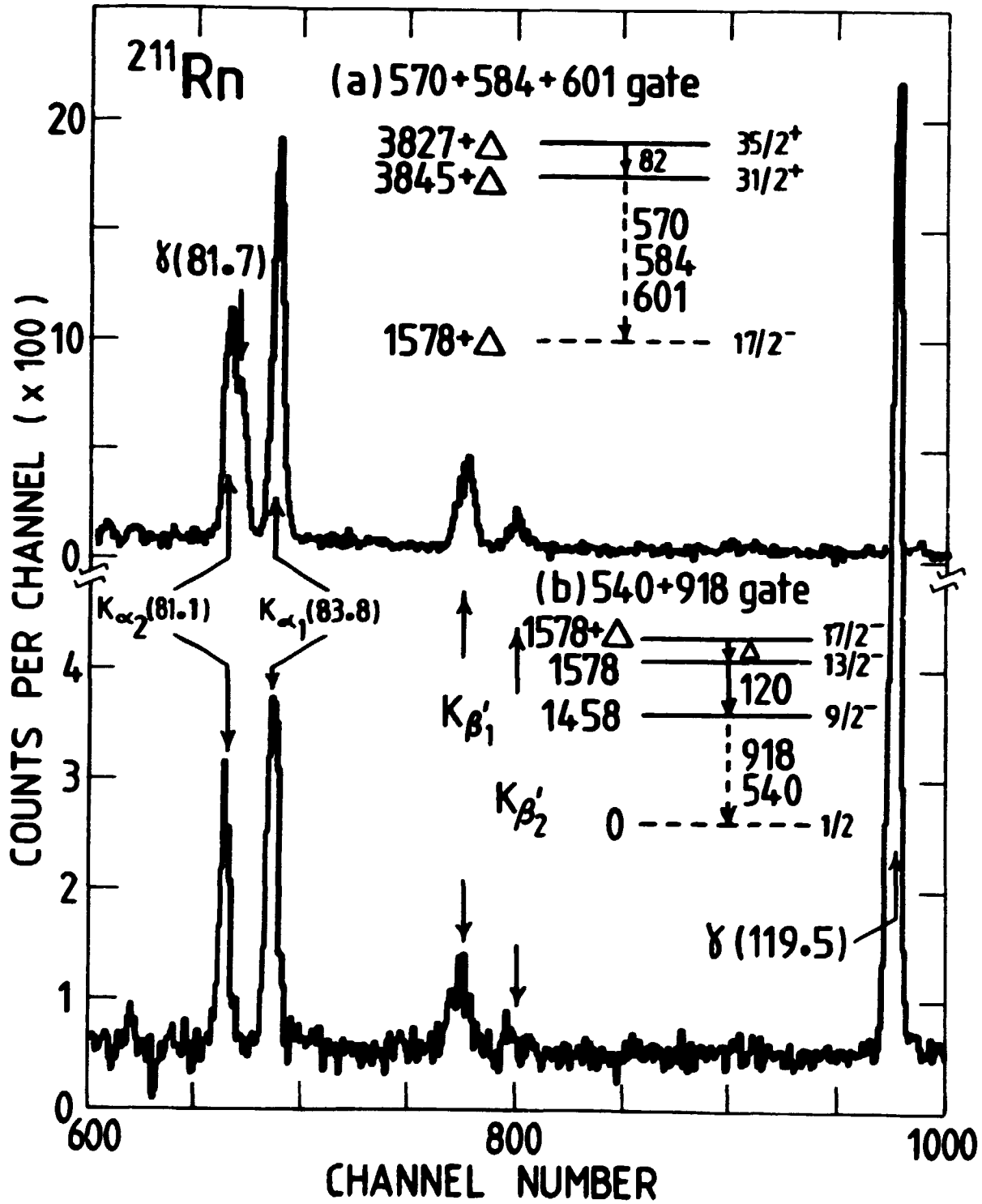
211Rn
(a) 570+584+601 gate
3827+Δ
3845+Δ
82
35/2+
31/2+
570
584
601
1578+Δ
17/2-
γ(81.7)
Kα2(81.1)
Kα1(83.8)
(b) 540+918 gate
1578+Δ
1578
1458
17/2-
13/2-
9/2-
120
918
540
0
1/2
Kβ'1
Kβ'2
γ(119.5)
COUNTS PER CHANNEL (x100)
CHANNEL NUMBER
0
1
2
3
4
10
20
600
800
1000

Fig. 2

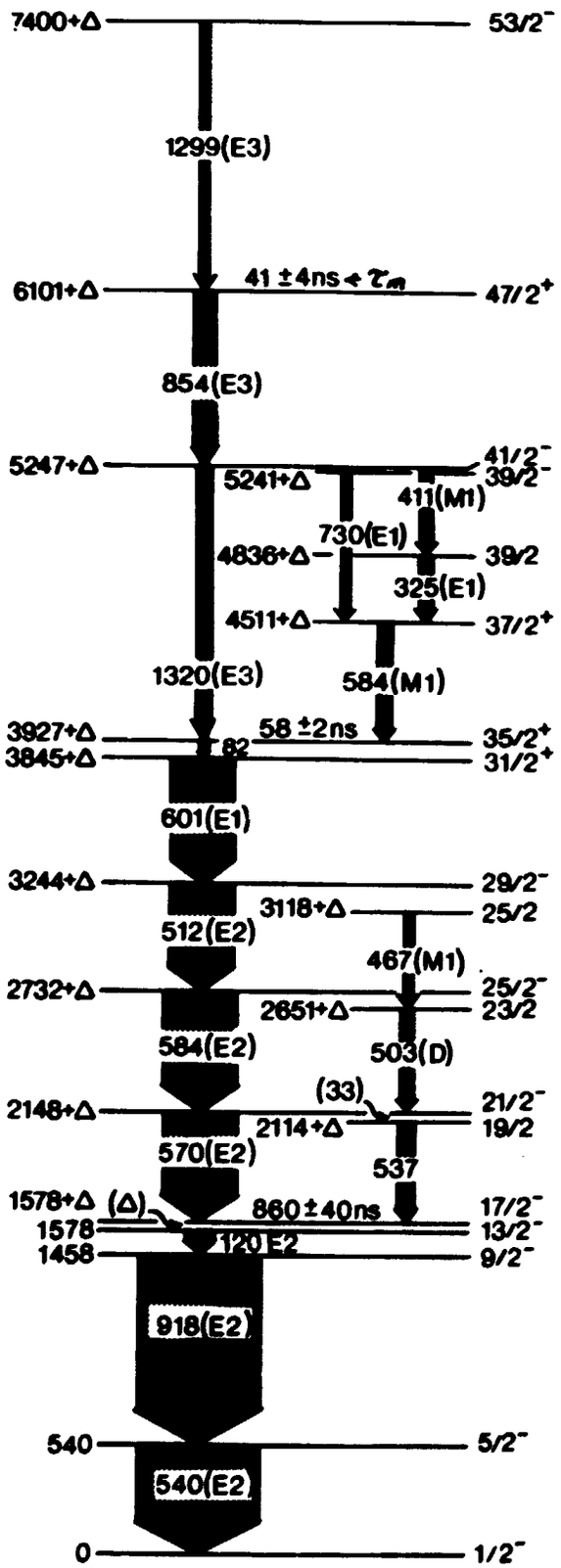
7400+Δ
53/2⁻
1299(E3)
6101+Δ
41 ±4ns
47/2⁺
854(E3)
5247+Δ
41/2⁻
5241+Δ
39/2⁻
411(M1)
730(E1)
4836+Δ
39/2
325(E1)
4511+Δ
37/2⁺
1320(E3)
584(M1)
3927+Δ
58 ±2ns
35/2⁺
3845+Δ
82
31/2⁺
601(E1)
3244+Δ
29/2⁻
3118+Δ
25/2
512(E2)
467(M1)
2732+Δ
25/2⁻
2651+Δ
23/2
584(E2)
503(D)
2148+Δ
(33)
21/2⁻
2114+Δ
19/2
570(E2)
537
1578+Δ
(Δ)
860 ±40ns
17/2⁻
1578
13/2⁻
1458
120 E2
9/2⁻
918(E2)
540
5/2⁻
540(E2)
0
1/2⁻

Fig. 3

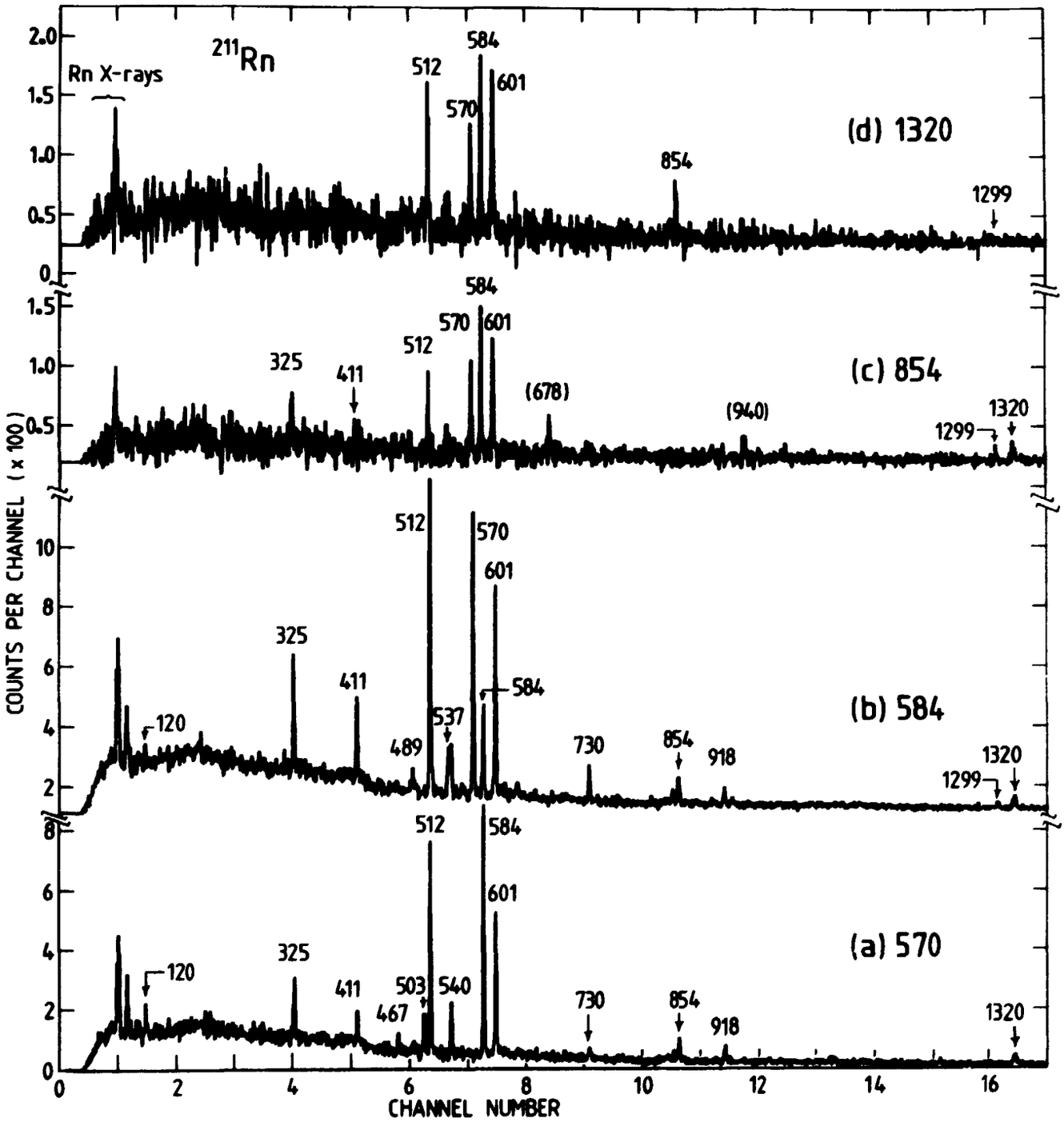
^{211}Rn
Rn X-rays
(d) 1320
(c) 854
(b) 584
(a) 570
COUNTS PER CHANNEL (x 100)
CHANNEL NUMBER
512
584
570
601
325
411
(678)
(940)
1299
1320
120
537
489
730
854
918
503
540
467
0
2
4
6
8
10
12
14
16

Fig. 4

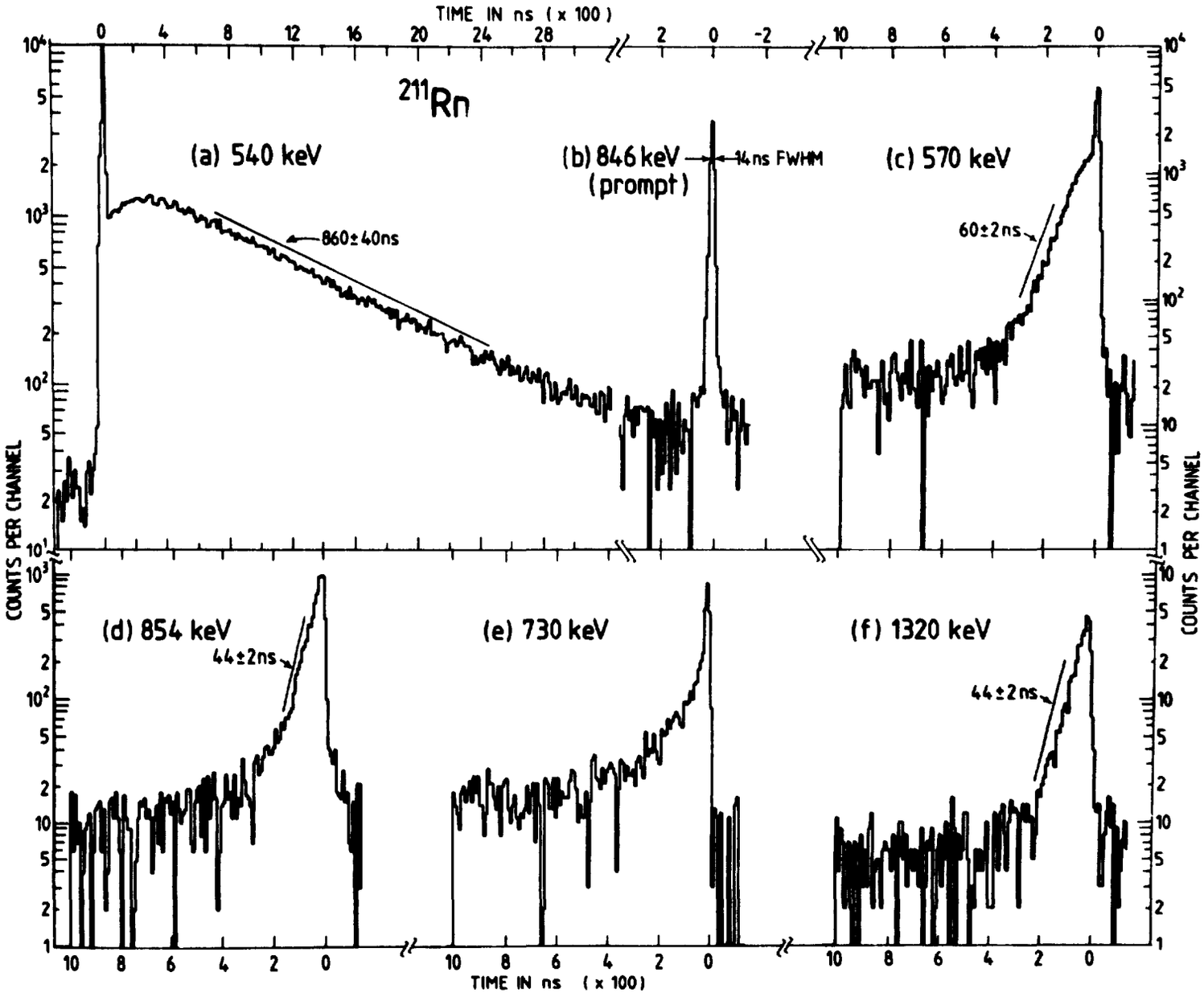
TIME IN ns (x 100)
^{211}Rn
(a) 540 keV
860±40ns
(b) 846 keV
(prompt)
14ns FWHM
(c) 570 keV
60±2ns
(d) 854 keV
44±2ns
(e) 730 keV
(f) 1320 keV
44±2ns
COUNTS PER CHANNEL
COUNTS PER CHANNEL
TIME IN ns (x 100)

Fig. 5

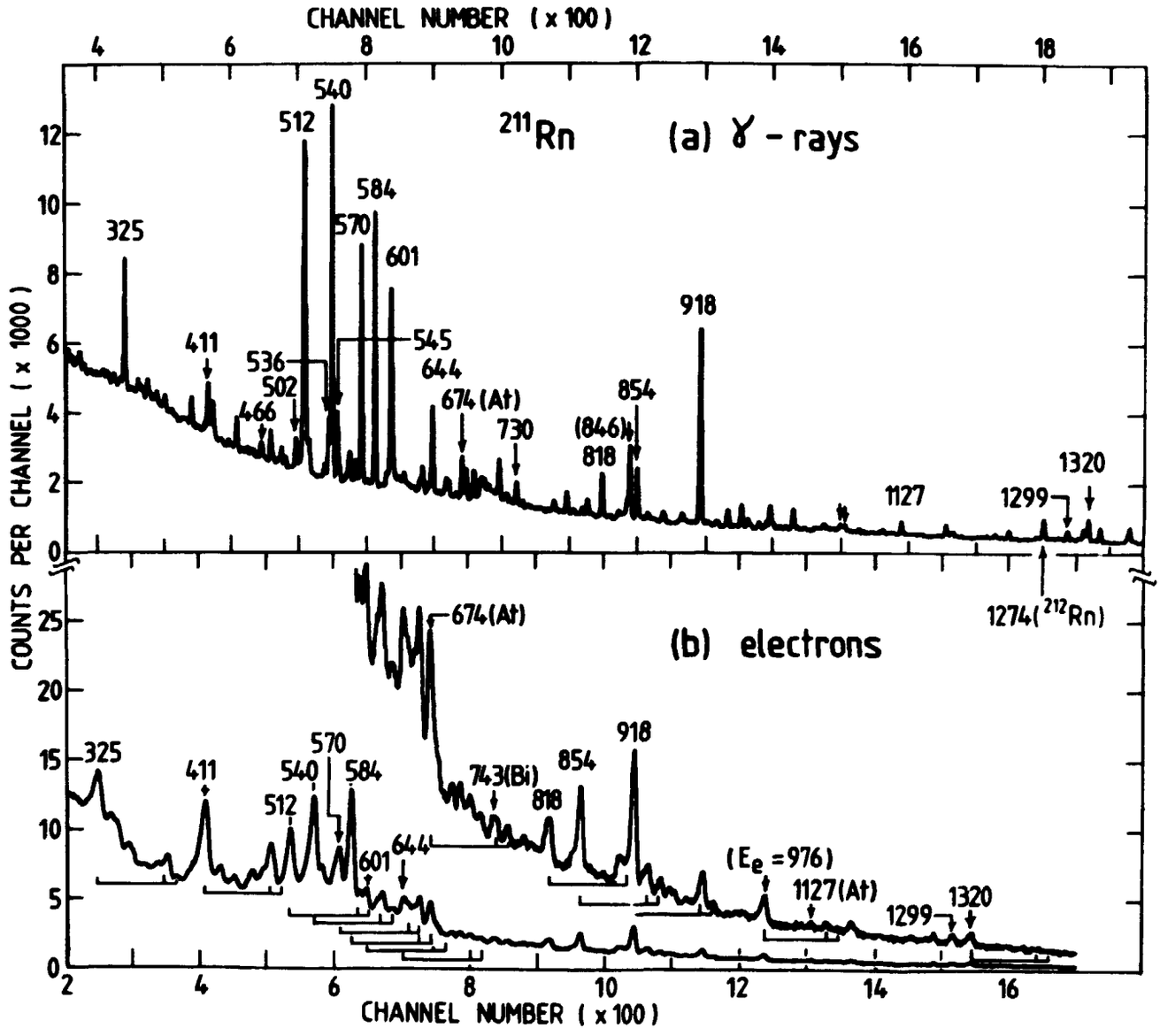
CHANNEL NUMBER (x 100)
^{211}Rn
(a) γ - rays
325
512
540
584
570
601
411
536
502
466
545
644
674 (At)
730
818
(846)
854
918
1127
1299
1320
1274 (^{212}Rn)
COUNTS PER CHANNEL (x 1000)
(b) electrons
674(At)
325
411
512
540
570
584
601
644
743(Bi)
818
854
918
(Eₑ = 976)
1127(At)
1299
1320
CHANNEL NUMBER (x 100)

Fig. 6

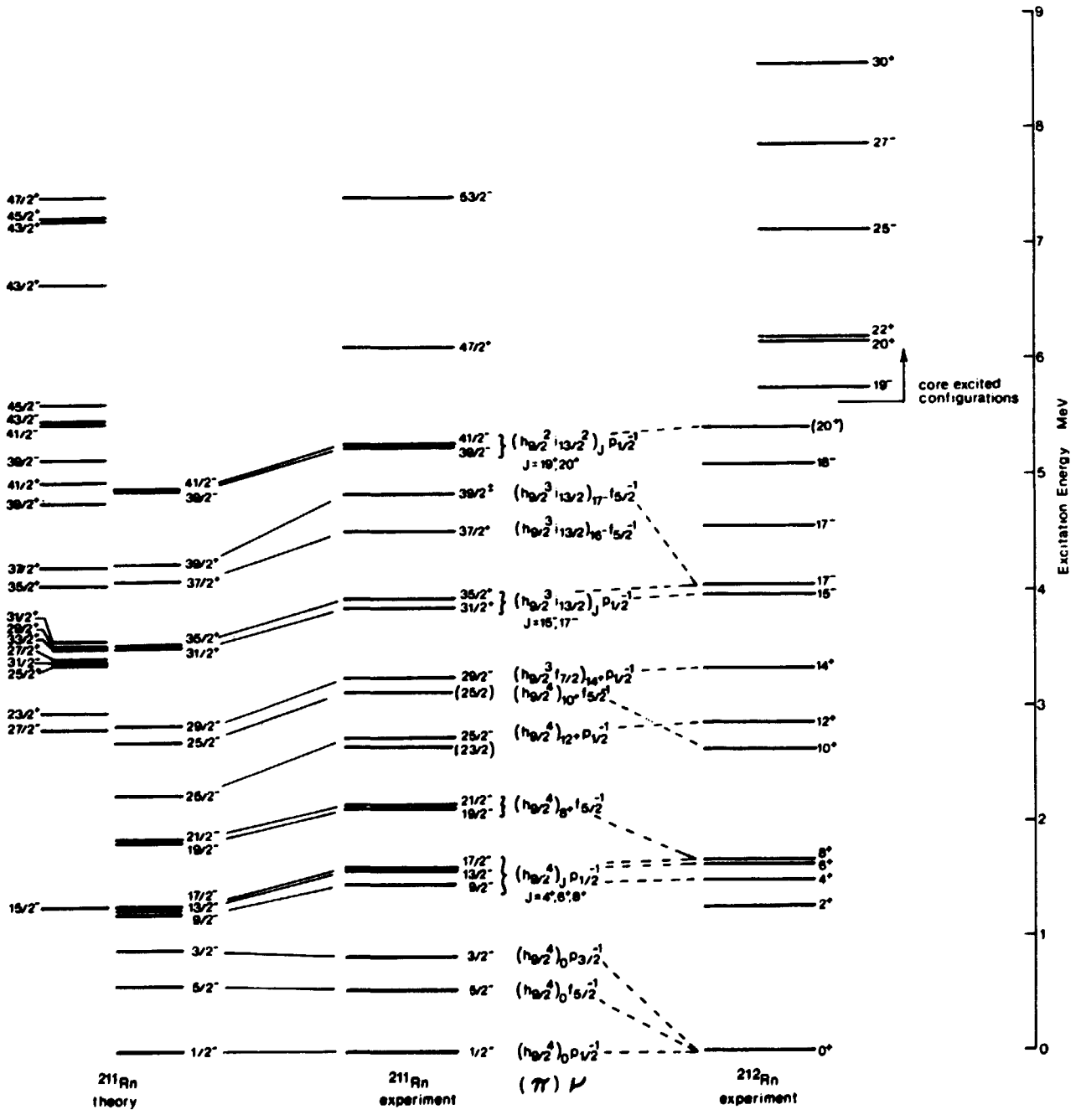
core excited configurations
Excitation Energy MeV
211Rn theory
211Rn experiment
(π) ν
212Rn experiment

Fig. 7

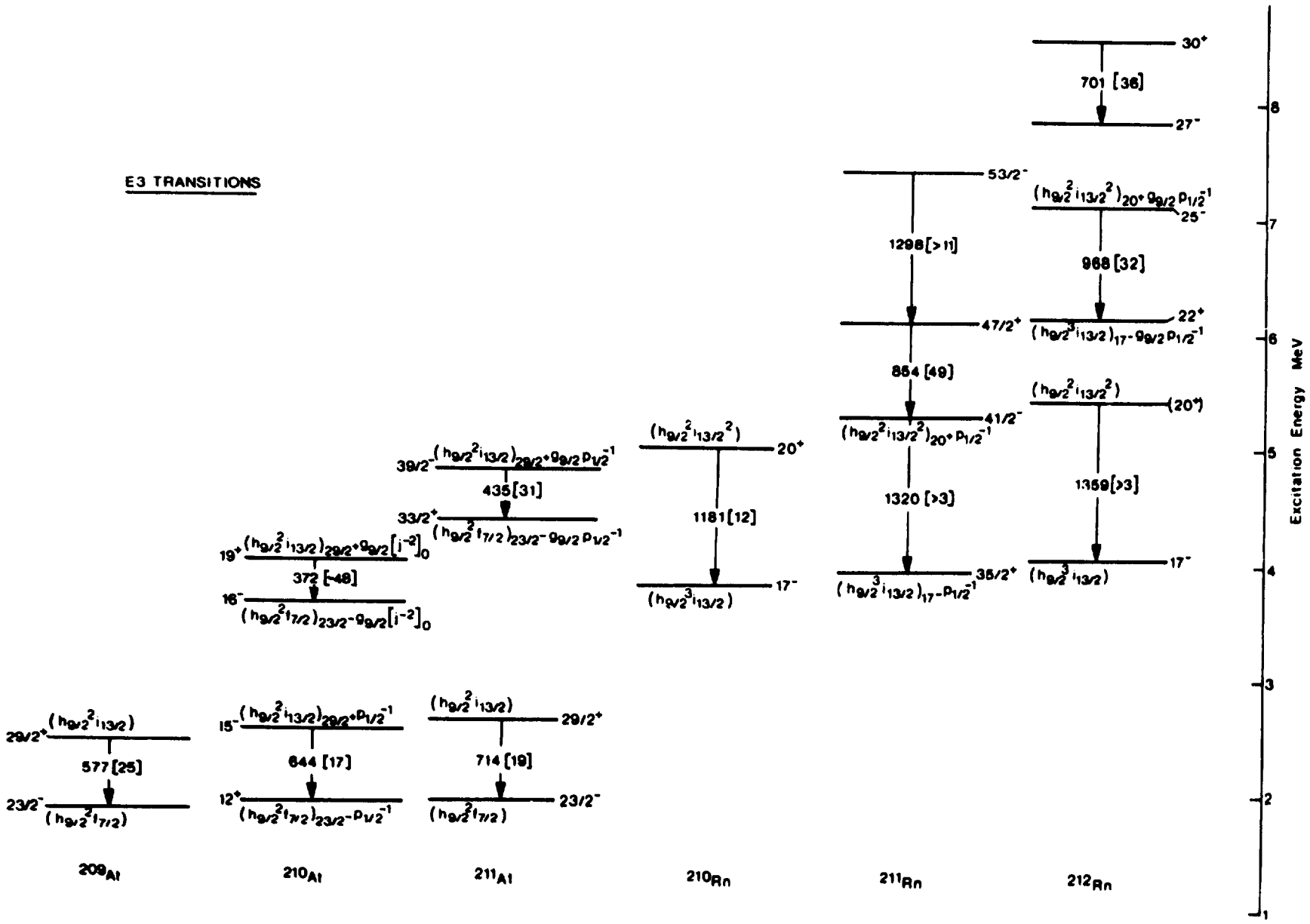
E3 TRANSITIONS
Excitation Energy MeV
1
2
3
4
5
6
7
8
209At
210At
211At
210Rn
211Rn
212Rn
29/2+ (h9/2² i13/2)
577 [25]
23/2- (h9/2² f7/2)
15- (h9/2² i13/2)29/2+ p1/2⁻¹
644 [17]
12+ (h9/2² f7/2)23/2- p1/2⁻¹
19+ (h9/2² i13/2)29/2+ g9/2 [i⁻²]0
372 [48]
16- (h9/2² f7/2)23/2- g9/2 [i⁻²]0
39/2- (h9/2² i13/2)29/2+ g9/2 p1/2⁻¹
435 [31]
33/2+ (h9/2² f7/2)23/2- g9/2 p1/2⁻¹
(h9/2² i13/2²) 20+
1181 [12]
17- (h9/2³ i13/2)
(h9/2² i13/2) 29/2+
714 [19]
23/2- (h9/2² f7/2)
53/2-
1298 [>11]
47/2+
854 [49]
41/2- (h9/2² i13/2²)20+ p1/2⁻¹
1320 [>3]
35/2+ (h9/2³ i13/2)17- p1/2⁻¹
30+
701 [36]
27-
(h9/2² i13/2²)20+ g9/2 p1/2⁻¹ 25-
968 [32]
22+ (h9/2³ i13/2)17- g9/2 p1/2⁻¹
(h9/2² i13/2²) (20+)
1359 [>3]
17- (h9/2³ i13/2)

Fig. 8

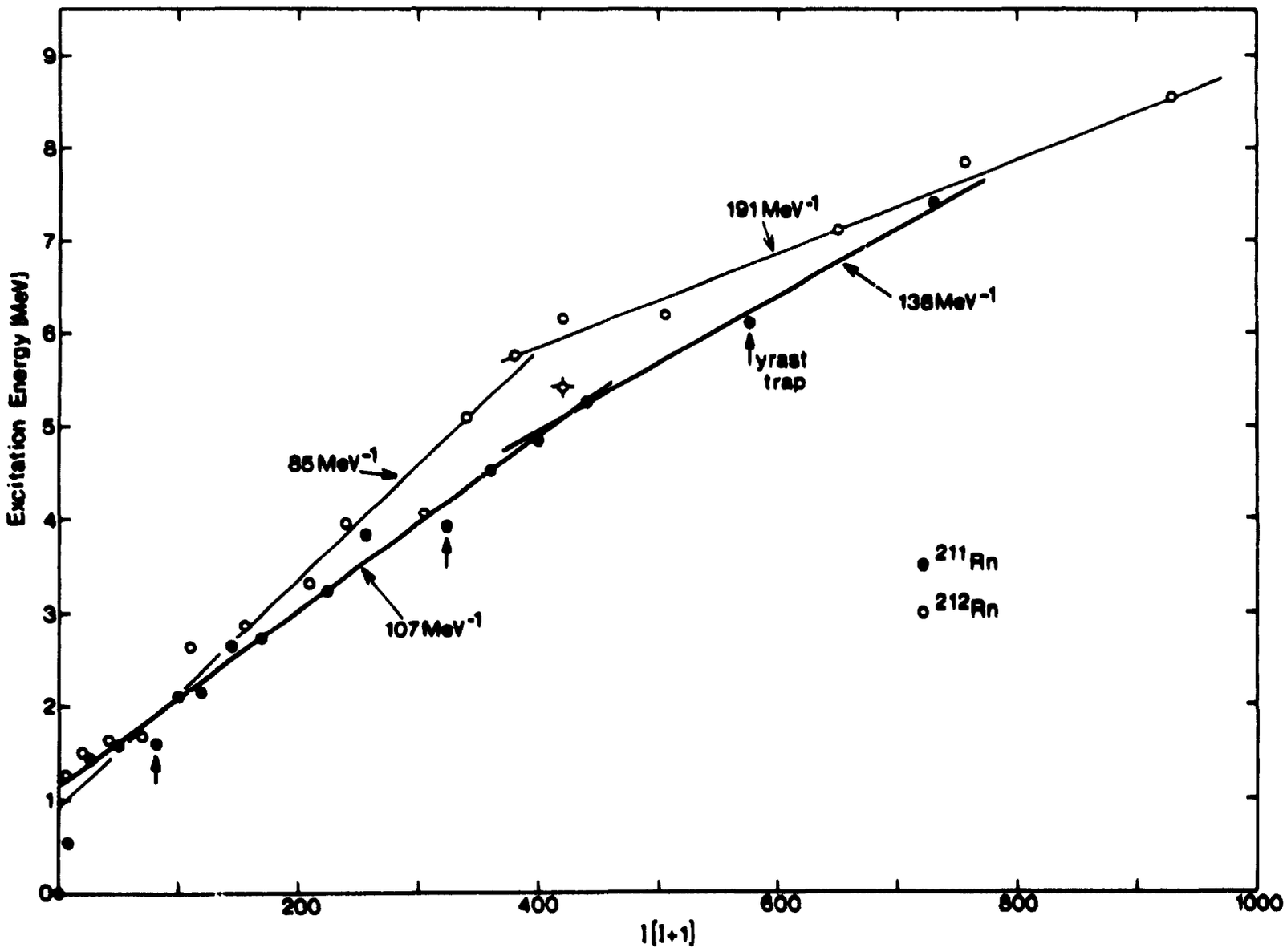
Excitation Energy (MeV)
I[I+1]
191 MeV⁻¹
138 MeV⁻¹
85 MeV⁻¹
107 MeV⁻¹
yrast trap
211Rn
212Rn
0
1
2
3
4
5
6
7
8
9
200
400
600
800
1000

Fig. 9